European Rotorcraft Forum

NONLINEAR OPTIMAL ADAPTIVE TRANSITION CONTROL OF A TOLT-PROP VTOL UAV

Murat Senipek *, muratsenipek@gmail.com
Metehan Yayla*, myayla@metu.edu.tr
Osman Gungor*, osman0gungor@gmail.com
Levent Cevher*, levent.cevher@gmail.com
Ali Turker Kutay*, kutay@metu.edu.tr
Ozan Tekinalp*, tekinalp@metu.edu.tr

Abstract
In this work, transition corridor determination and transition control of a Tilt-Prop Vertical Takeoff and Landing aircraft problem is addressed. Non-linear flight dynamics model of the aircraft is generated using the software Generic Air Vehicle Model. Transition corridor is estimated by using the constructed model and analyzed in terms of power consumption and flight efficiency. Automatic transition flight control system deals with fully automated transition control of Tilt-Prop UAV including uncertainties in system modeling and system parameters. Control system is integrated to a 6-DoF simulation environment. Different transition maneuvers are performed and results are discussed in terms of power consumption and efficiency. Efficiency of the transition controller is illustrated through simulations over the determined transition corridor. It is planned to integrate the nonlinear adaptive transition controller to the flight computer of the aircraft to validate the transition corridor with flight tests and perform automated transition to forward flight.

1. NOTATION

Notation used in this paper is fairly standard. Specifically, c_α and s_α (resp.) correspond to $\cos(\alpha)$ and $\sin(\alpha)$ (resp.), $\mathcal{F}_b = \mathcal{F}_b\left(C; u_1^{(b)}, u_2^{(b)}, u_3^{(b)}\right)$ describes the frame $\mathcal{F}_b$ which has the origin at point C and right-handed orthonormal unit vectors $u_i^{(b)}$'s, $u_j^{(m)}$ denotes the j^{th} unit vector of frame $\mathcal{F}_m$,

2. INTRODUCTION

Tilt rotor aircrafts may operate in wide range of airspeeds as they achieve a steady state flight condition. Tilt rotor aircrafts have the opportunity to generate lifting force both by the vertical components of propellers and the lift generated by the wing surfaces. Therefore, it results in multiple trim conditions in terms of tilt angle and angle of attack for a given forward velocity. Tilting capability enables the aircraft to be trimmed in multiple angle of attack values by setting a proper rotor tilt angle and RPM.

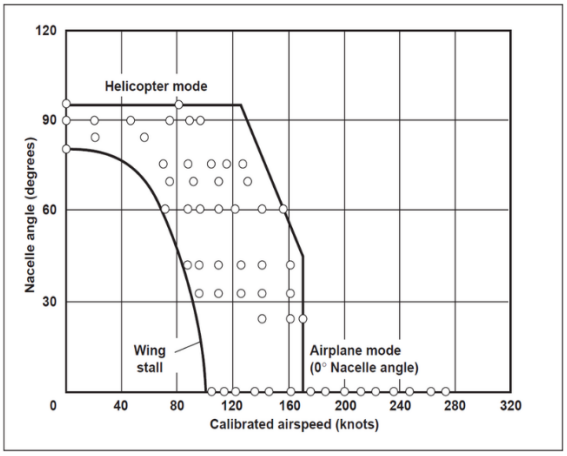

Figure 1: Conversion corridor of the XV-15 tilt rotor research aircraft[1]

Transition or conversion corridor defines the possible combinations of forward speed and rotor/propeller tilt angle as shown as a sample in Figure 1. In helicopter mode, tilt angle is 90 degrees and can be changed about ± 5 degrees according to the flapping capabilities of the aircraft. In

*Department of Aerospace Engineering, Middle East Technical University, Ankara, Turkey

airplane mode the tilt angle is 0 degrees and the airspeed is bounded by the stall speed and maximum speed. Between these two modes, it is called as transition flight and its envelope is illustrated by the conversion corridor. Lower airspeed part of the conversion corridor belongs to the high body pitch angle and limited by the wing stall, on the other hand upper bound of the conversion corridor is limited by the available power or propeller pitch. Between these two bounds, steady flight may be sustained. Choice of the type of transition flight depends on the requirements such as comfort, time or power consumption. Therefore, conversion corridor includes several information and benefits according to the mission requirements if the transition regime is analyzed in detail.

By the nature of all kind of UAVS, there are strong couplings in translational and rotational motions. In addition, highly nonlinear system dynamics, uncertainties in the system modeling, presence of unmodeled dynamics, external disturbances, and possible structural failures makes the controller design more and more difficult. Hence, advanced control strategies such as robust control and adaptive control becomes necessary. In the literature, there exist many flight control solutions for several types of HUAVs including tail-sitters[2,3,4], quad-tilt wing UAVs[5,6,7,8,9], and tricopter HUAVs[10,11,12,13,14,15].

Specifically, Chao et al[12] proposed a dynamic inversion based controller only for vertical flight (hover) mode, Casau et al[16] employed Linear Quadratic Regulator (LQR) controller for hover mode and forward flight (level flight) mode, Apkarian[9] proposed a linear cascade controller, P/PD/PID controller are used in several studies[6,11,10,15,17], Lyapunov based transition control is proposed by Flores and Lozano[18] where they added pitch dynamics in their next study[7], Li et al[4] proposed a Model Predictive Control for hover mode, Liu et al[5] are introduced a multi-model adaptive control (MMAC) approach for transition maneuver, a unified hierarchical control approach with PID based attitude controller for all flight modes is introduced by Lyu[2] et al while the position controllers for level flight mode and hover mode are adopted from Ref[19] and Ref[20] (resp.), Oznalbant[21] et al are employed PID based three individual control strategies for all three flight modes, Yeo[22] et al introduced linear controller for altitude control whereas Lyapunov-based nonlinear control is employed in attitude control for their hierarchical control scheme, and sequential loop control with adaptive control theory is introduced by Yildiz[8] et al. Further discussions on control techniques of HUAVs can be found in review papers of Ref[23], and references therein.

Except from the control solution proposed by Hartmann[14] et al, all the studies referenced up to here divide control problem into three discrete flight modes; that is a controller is designed for every discrete aircraft configurations such as vertical flight, transition maneuver, and forward flight modes. Furthermore, they perform the transition maneuver with a discrete and instantaneous change in tilting mechanisms. However, Hartmann[14] do not consider the uncertainties in their controller design. On the other hand, Yildiz[8] et al takes the uncertainties into account in their controller design while the transition maneuver takes place by switching between tilt angles of 0^o, 20^o, 70^o, 90^o.

In this work, mathematical study of transition corridor determination and adaptive control of Tilt-prop VTOL UAV for all flight modes including hover, vertical flight, and forward flight is conducted. Approximately 5 kg scale mini Tilt-prop UAV as given in Table 3 is designed, and manufactured under the ongoing work in Middle East Technical University (METU) Aerospace Engineering Department[24]. The nonlinear flight dynamics model of the aircraft is generated by using the Generic Air Vehicle Model (GAVM) software which is an object oriented non-linear flight simulation model[25]. The transition corridor is determined by using GAVM. When dealing with control of the aircraft, we obtain a unified control strategy for all the flight modes (including takeoff, vertical flight, hover, forward flight, and landing) of a vertical takeoff and landing capable fixed-wing unmanned aerial vehicle. In the outer loop, Lyapunov-based control is employed whereas adaptive controller is developed in the inner loop control. Furthermore, a control allocation strategy is proposed. Thus, unified controller for all flight modes is achieved. Simulations are performed to show the efficacy of the adaptive flight controller. In addition, transition maneuvers are simulated for both wings level transition and efficient transition. Simulation results are compared with the conversion corridor which is generated by GAVM and results are discussed.

3. TILT-PROP VTOL UAV

Aircraft is a tricopter configuration with fixed swept-back wings. In hover mode aircraft is controlled by RPM of three propellers and rear motor tilt angle. In hover, yaw moment is balanced

by the aft motor tilt in roll axis. Transition is done by tilting the front motors down and reducing the RPM of aft motor. In forward flight mode it is a twin propeller flying wing configuration with throttle, aileron, and elevator inputs. Aileron and elevator commands are provided by elevons with differential and collective tilting of control surfaces. Hover and forward flight configurations are illustrated in Figure 2 and Figure 3.

The aircraft had successfully completed hovering flight tests in tricopter configuration[24]. The design has been improved as a swept back configuration for transition and forward flight[26],[27]. In current status, wind tunnel tests, flight tests in hover mode and transition wind tunnel tests are conducted.

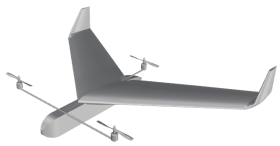

Figure 2: Hovering Flight Configuration

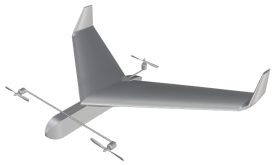

Figure 3: Forward Flight Configuration

Aircraft specifications are provided in Table 1. In hover yaw moment is balanced by the aft motor tilt in roll axis. During the transition phase front motors are tilted in pitch axis and back motor is used to provide aircraft stability. In forward flight aft motor is stopped and aircraft operates as twin propeller swept back configuration with active elevons and rudders.

Characteristic	
Wingspan	$1.6m$
Wing Area	$0.63m^2$
Mean Aerodynamic Chord	$0.33m$
Sweep Angle	39^o
Taper Ratio	0.55
Motors	3x Scorpion S3020
Max. T/O Weight	$4.9kg$ ($1kg$ payload)
Engine Power	4S 10000 mAh Li-Po

Table 1: Tilt-Rotor Tricopter UAV Specifications

4. NONLINEAR MODEL

The nonlinear trim and simulation model is generated by using the Generic Air Vehicle Model (GAVM). GAVM is a generic and object oriented rotorcraft modeling, design, analysis and simulation software[25]. Although GAVM was firstly developed for conventional helicopters it is validated for aircraft and tilt rotor air vehicles. GAVM is designed to solve problems in aerodynamics, performance and control. In GAVM there are several sub-components which exist in air vehicles such as rotor, propeller, wing and fuselage. The propeller models include a validated modified version of the theory of QPROP which incorporates the blade element/vortex formulation of the open-source code QPROP and viscous airfoil data[28]. Available control inputs for propeller object are longitudinal and lateral tilt angles, blade pitch angle and blade angular velocity. Rotor Model includes a rigid rotor model with finite state dynamic inflow models and second order coupled flapping and lagging dynamics. Wing Model provides two types of aerodynamic modeling of the wing. First one is the second order lifting line theory which includes viscous airfoil data and applicable to swept wings and second one is the table-lookup methodology for 6-DOF aerodynamic coefficients. Control surface inputs may be defined as tables or linear coefficients of 6-DOF forces and moments. By using the ControlAllocation class each input may be coupled, related or de/activated as desired. Therefore, reduction of input sets is possible. GAVM is utilized for tricopter tilt rotor configuration. In GAVM each sub component of the aircraft is modeled separately and mainly three propeller and four wing objects are defined and connected into the fuselage as illustrated in Figure 4. Propellers have RPM and tilt angle inputs and

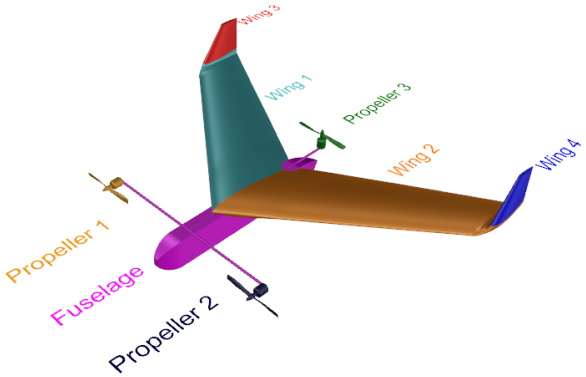

Figure 4: GAVM Components Utilized in Nonlinear Model

wings have control surfaces of elevons. Front motors has a common tilt angle.

Since this UAV is designed to operate both in hover and forward flight, the aerodynamic properties of the wing, fuselage and control surfaces should be predicted with sufficient accuracy. Wing-body aerodynamics are modeled by 3-D panel method and 3-D viscous CFD as given in Figure 5 and Figure 6. 3-D panel method mainly

employed to predict the aerodynamic control derivatives for rudder, elevator and aileron commands. Panel solutions are obtained for deflected aileron, elevator and rudder configurations and linear interpolation is performed to obtain the control derivatives.

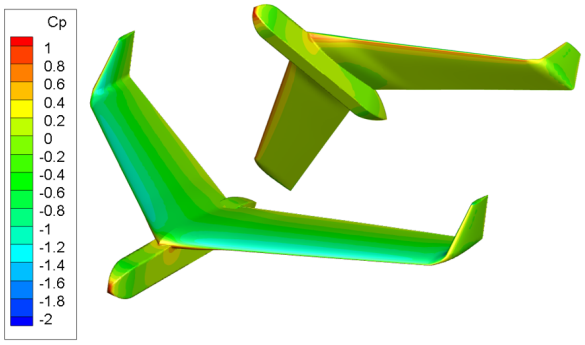

Figure 5: GAVM Components Utilized in Nonlinear Model

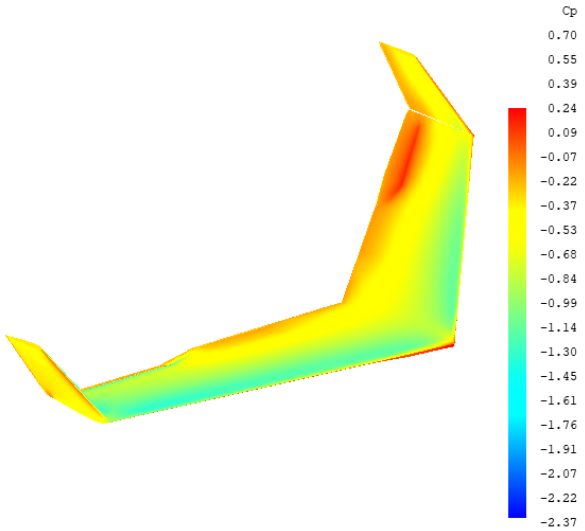

Figure 6: GAVM Components Utilized in Nonlinear Model

The procedure of calculating control moments generated for a given elevator deflection angle may be observed from Figure 7. In the figure the pitch moment coefficient versus angle of attack curves for two different elevator deflection angles are shown. The associated pitching moment coefficient is then calculated at zero degree angle of attack and used in the simulation. All linearized control moments are obtained by using this approximation. In calculating control moments coefficients related to the control surface deflections, it is assumed that elevator deflection is directly associated with pitch moment, rudder is

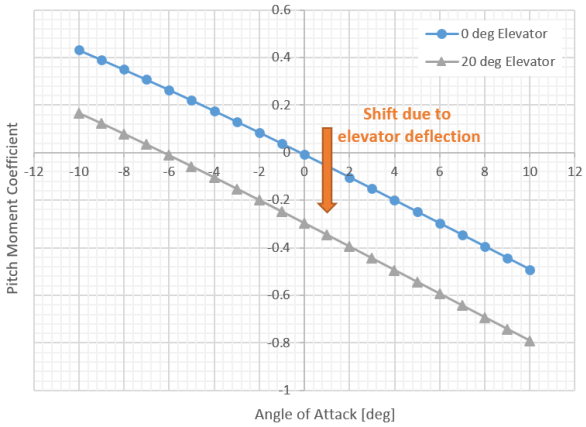

Figure 7: Shift in pitch moment due to a deflected elevator

associated with yaw moment and ailerons are associated with roll moment similarly. Coupling effects and unsteady loads are neglected. In addition, interference between the propeller wake and wing-body is neglected.

CFD is mainly used to predict stall behavior and viscous drag. Sideslip and angle of attack sweeps are conducted to integrate the aerodynamic coefficients as 6-DOF aerodynamic loads table into GAVM. In CFD analyses propeller wake and wing interaction is neglected.

5. SYSTEM DESCRIPTION

In this section, we describe dynamics of the Tilt-prop VTOL UAV (TP-UAV). Reference frames are denoted as

$$\mathcal{F}_o = \mathcal{F}_o\left(O; u_1^{(o)}, u_2^{(o)}, u_3^{(o)}\right)$$
$$\mathcal{F}_b = \mathcal{F}_b\left(C; u_1^{(b)}, u_2^{(b)}, u_3^{(b)}\right)$$
$$\mathcal{F}_a = \mathcal{F}_a\left(C; u_1^{(a)}, u_2^{(a)}, u_3^{(a)}\right)$$
$$\mathcal{F}_{r_i} = \mathcal{F}_{r_i}\left(R_i; u_1^{(r_i)}, u_2^{(r_i)}, u_3^{(r_i)}\right).$$

where $\mathcal{F}_b$ is aircraft body frame, $\mathcal{F}_o$ is inertial frame (Earth is assumed non-rotating and flat), $\mathcal{F}_a$ is stability axis, and $\mathcal{F}_{r_i}$ for $i = 1, 2, 3$ are motor frames. Note that body frame $\mathcal{F}_b$ and motor frames $\mathcal{F}_{r_i}$ for $i = 1, 2, 3$ are illustrated in Figure 8 and Figure 9, respectively.
When modeling the aircraft dynamics, we consider

- Propulsive forces, $\boldsymbol{F}_{th}$
- Aerodynamic forces (Drag, Lift), $\boldsymbol{F}_{aero}$
- Gravitational force, $\boldsymbol{F}_g$

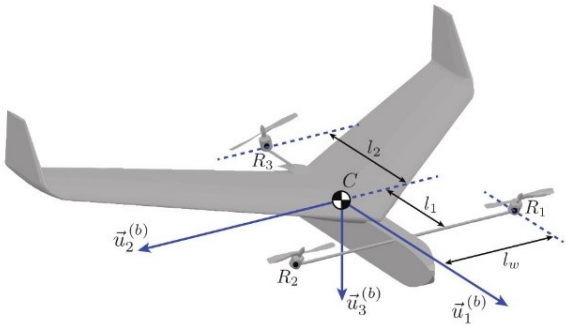

Figure 8: Reference Frames

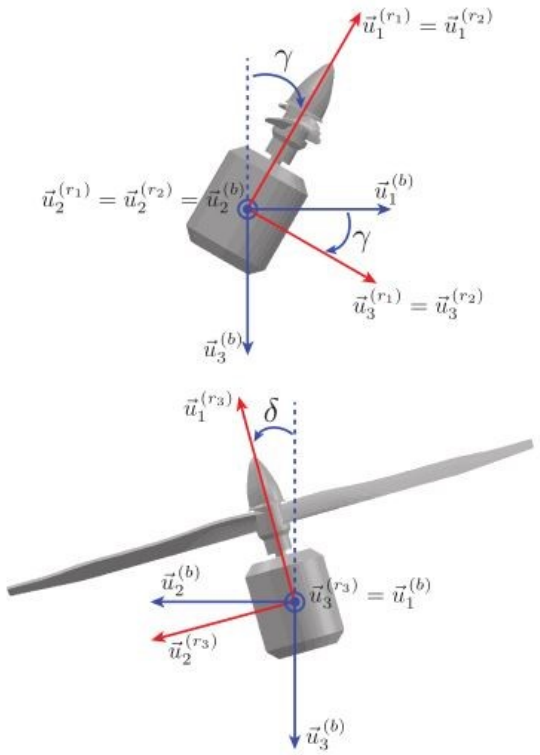

Figure 9: Motor Frames

as well as

- Moment due to rotor forces, $\boldsymbol{M}_{th}$
- Aerodynamic moments, $\boldsymbol{M}_{aero}$
- Motor torques, $\boldsymbol{Q}_m$
- Moments due to control surface deflections (aileron, elevator), $\boldsymbol{M}_{ctrl}$.

5.1. Translational Equations of Motion

Propulsive forces expressed in the body frame $\mathcal{F}_b$ are modeled as

$$\boldsymbol{F}_{th} = \begin{bmatrix} c_{tf} s_\gamma \left(\omega_1^2 + \omega_2^2\right) \\ c_{ta} \omega_3^2 s_\delta \\ -c_{tf} c_\gamma \left(\omega_1^2 + \omega_2^2\right) - c_{ta} c_\delta \omega_3^2 \end{bmatrix} \tag{1}$$

where c_{tf} and c_{ta} are thrust coefficients for front and aft motors (resp.), $omega_i$ are angular velocity of i^{th} motor for $i = 1, 2, 3$, γ is front motor tilt angle and δ is aft motor tilt angle.

Aerodynamic forces expressed in body frame $\mathcal{F}_b$ are given by

$$\boldsymbol{F}_{aero} = \begin{bmatrix} -F_{\text{drag}} c_\alpha + F_{\text{lift}} s_\alpha \\ 0 \\ -F_{\text{drag}} s_\alpha - F_{\text{lift}} c_\alpha \end{bmatrix} \tag{2}$$

with F_{drag} and F_{lift} being

$$\begin{aligned} F_{\text{drag}} &= \frac{1}{2} \rho_\infty V_\infty^2 S_{ref} C_D \\ F_{\text{lift}} &= \frac{1}{2} \rho_\infty V_\infty^2 S_{ref} C_L \end{aligned} \tag{3}$$

where C_L and C_D are lift and drag coefficients (resp.), α is the angle of attack, S_{ref} is reference wing area, ρ_∞ is the air density at the flight altitude and V_∞ is the true airspeed of the aircraft.

Gravitational force expressed in body frame $\mathcal{F}_b$ becomes

$$\boldsymbol{F}_g = \begin{bmatrix} -mgs_\theta \\ mgs_\phi c_\theta \\ mgc_\phi c_\theta \end{bmatrix} \tag{4}$$

where m is mass of the aircraft, g is gravitational acceleration, ϕ and θ (resp.) are roll and pitch attitude angles (resp.) of the aircraft. Then, translational equations of motion written in body frame are obtained as in Equation 5.

$$\begin{aligned} \dot{u} =& \frac{1}{m} \left[c_{tf} s_\gamma \left(\omega_1^2 + \omega_2^2\right) - F_{\text{drag}} c_\alpha \right. \\ & \left. + F_{\text{lift}} s_\alpha - mgs_\theta \right] + rv - qw \\ \dot{v} =& \frac{1}{m} \left[c_{ta} \omega_3^2 s_\delta + mgs_\phi c_\theta \right] + pw - ru \\ \dot{w} =& \frac{1}{m} \left[-c_{tf} c_\gamma \left(\omega_1^2 + \omega_2^2\right) - c_{ta} c_\delta \omega_3^2 \right. \\ & \left. - F_{\text{drag}} s_\alpha - F_{\text{lift}} c_\alpha + mgc_\phi c_\theta \right] + qu - pv \end{aligned} \tag{5}$$

where u, v, w are aircraft velocity components in body frame and p, q, r are Euler rates.

5.2. Rotational Equations of Motion

Now, we derive the rotational equations of motion using Euler's equation

$$\widehat{\boldsymbol{J}}^{(b)} \begin{bmatrix} \dot{p} \\ \dot{q} \\ \dot{r} \end{bmatrix} + \begin{bmatrix} 0 & -r & q \\ r & 0 & -p \\ -q & p & 0 \end{bmatrix} \widehat{\boldsymbol{J}}^{(b)} \begin{bmatrix} p \\ q \\ r \end{bmatrix} = \boldsymbol{M}_{tot} \tag{6}$$

where $\widehat{\boldsymbol{J}}^{(b)}$ is the matrix representation of inertia tensor in body frame $\mathcal{F}_b$. Total moment acting on the aircraft is

$$\boldsymbol{M}_{tot} = \boldsymbol{M}_{th} + \boldsymbol{Q}_m + \boldsymbol{M}_{aero} + \boldsymbol{M}_{ctrl} \tag{7}$$

Moment due to rotor forces expressed in body frame is

$$\boldsymbol{M}_{th} = \begin{bmatrix} c_{tf} l_w \left(\omega_1^2 - \omega_2^2\right) c_\gamma \\ c_{tf} l_1 \left(\omega_1^2 + \omega_2^2\right) c_\gamma - c_{ta} l_2 \omega_3^2 c_\delta \\ c_{tf} l_w \left(\omega_1^2 - \omega_2^2\right) s_\gamma - c_{ta} l_2 \omega_3^2 s_\delta \end{bmatrix} \tag{8}$$

where distances l_1, l_2, and l_w are as in Figure 8.

Rotor torque vector is represented in body frame $\mathcal{F}_b$ as

$$\boldsymbol{Q}_m = \begin{bmatrix} -c_{qf} \left(\omega_1^2 - \omega_2^2\right) s_\gamma \\ -c_{qa} \omega_3^2 s_\delta \\ c_{qf} \left(\omega_1^2 - \omega_2^2\right) c_\gamma + c_{qa} \omega_3^2 c_\delta \end{bmatrix} \tag{9}$$

All the aerodynamic moments but pitching moment are neglected. Panel method is used to estimate the moment coefficients of the aircraft. Using the non-dimensional pitching moment coefficient C_{M_y} given in Figure 10, aerodynamic moment $\boldsymbol{M}_{aero}$ can be expressed in body frame $\mathcal{F}_b$ as

$$\boldsymbol{M}_{aero} = \begin{bmatrix} 0 \\ M_{pitch} \\ 0 \end{bmatrix} \tag{10}$$

where

$$M_{pitch} = \frac{1}{2} \rho_\infty V_\infty^2 S_{ref} \bar{c} C_{M_y} \tag{11}$$

with $\bar{c}$ being mean aerodynamic chord.

We consider elevator and aileron deflections for attitude control. For the yaw motion, control input is the aft rotor tilt angle. Thus, we do not need rudder in the design. Considering these, moment vector due to control surfaces can be expressed as

$$\begin{aligned} \boldsymbol{M}_{ctrl} &= \begin{bmatrix} M_{x,a} \\ M_{y,e} \\ 0 \end{bmatrix} \\ M_{y,e} &= \frac{1}{2} \rho_\infty V_\infty^2 S_{ref} \bar{c}\, C_{M_e} \delta_e \\ M_{x,a} &= \frac{1}{2} \rho_\infty V_\infty^2 S_{ref} \bar{c}\, C_{M_a} \delta_a \end{aligned} \tag{12}$$

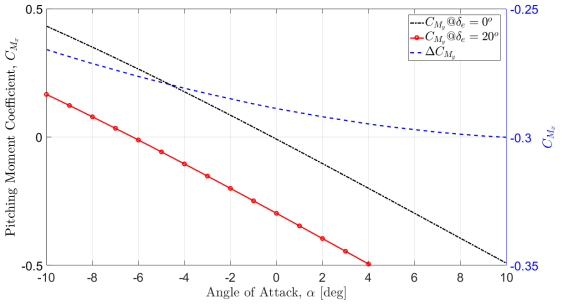

Figure 10: Pitching moment coefficient variation with angle of attack

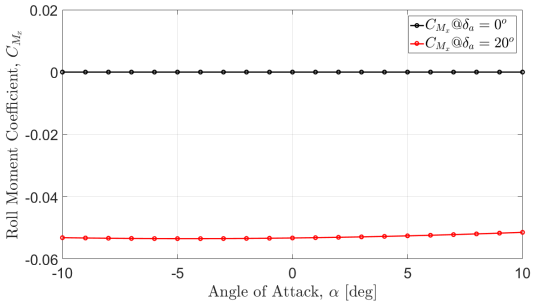

Figure 11: Roll moment coefficient variation with angle of attack

where $M_{y,e}$ is the additional pitching moment due to elevator deflection and $M_{x,a}$ is the additional rolling moment due to aileron deflection. Assuming the additional pitching (rolling) moment due to elevator (aileron) deflection is linear with respect to elevator (aileron) deflection angle up to 10 degrees, we can obtain C_{M_e} (C_{M_a}) using Figure 10 (Figure 11) as $C_{M_e} = 0.82$ ($C_{M_a} = 0.15$).

Finally, rotational equations of motion becomes

$$\begin{aligned} \dot{p} =& \frac{1}{I_x} \left[c_{tf} l_w \left(\omega_1^2 - \omega_2^2\right) c_\gamma - c_{qf} \left(\omega_1^2 - \omega_2^2\right) s_\gamma \right. \\ & \left. + M_{gyro,1} + M_{x,a} + qr \left(I_y - I_z\right) \right] \\ \dot{q} =& \frac{1}{I_y} \left[c_{tf} l_1 \left(\omega_1^2 + \omega_2^2\right) c_\gamma - c_{ta} l_2 \omega_3^2 c_\delta - c_{qa} \omega_3^2 s_\delta \right. \\ & \left. + M_{gyro,2} + M_{pitch} + M_{y,e} + pr \left(I_z - I_x\right) \right] \\ \dot{r} =& \frac{1}{I_z} \left[c_{tf} l_w \left(\omega_1^2 - \omega_2^2\right) s_\gamma - c_{ta} l_2 \omega_3^2 s_\delta + c_{qa} \omega_3^2 c_\delta \right. \\ & \left. + c_{qf} \left(\omega_1^2 - \omega_2^2\right) c_\gamma + M_{gyro,3} + qp \left(I_x - I_y\right) \right] \end{aligned} \tag{13}$$

6. CONTROLLER DESIGN

In this section, we describe the controller design for a Tilt-prop VTOL UAV. In the proposed hierarchical approach, pilot generated inertial position is translated to desired body velocities through a navigation algorithm with a

PD-controller inside. Then, in order to track the desired velocities, an outer-loop controller is designed via Lyapunov-based approach. Next, desired attitude commands and front motor tilt angle are fed into inner loop controller which is designed using model reference adaptive control theory. With control allocation and mixer algorithms, all three motor RPM commands, control surface deflections and motor tilt angles are determined. Proposed control architecture is illustrated in Figure 12.

6.1. Inner Loop Controller Design

For simplicity, we define the followings

$$
\begin{aligned}
u_1 &\triangleq \omega_1^2 - \omega_2^2, \qquad u_2 \triangleq \omega_1^2 + \omega_2^2 \\
u_3 &\triangleq \omega_3^2 c_\delta, \qquad u_4 \triangleq \omega_3^2 s_\delta \\
U_\phi &\triangleq c_{tf} l_w u_1 c_\gamma - c_{qf} u_1 s_\gamma + M_{x,a} \\
U_\theta &\triangleq c_{tf} l_1 u_2 c_\gamma - c_{ta} l_2 u_3 - c_{qa} u_4 + M_{y,e} \\
U_\psi &\triangleq c_{tf} l_w u_1 s_\gamma - c_{ta} l_2 u_4 + c_{qf} u_1 c_\gamma + c_{qa} u_3 \\
U_z &\triangleq -c_{tf} u_2 c_\gamma - c_{ta} u_3
\end{aligned} \tag{14}
$$

Then, equations of motion become

$$
\begin{aligned}
\ddot{\phi} \cong \dot{p} &= \frac{1}{I_x}\left[M_{gyro,1} + qr\left(I_y - I_z\right)\right] + \frac{1}{I_x} U_\phi \\
\ddot{\theta} \cong \dot{q} &= \frac{1}{I_y}\left[M_{gyro,2} + M_{pitch} + pr\left(I_z - I_x\right)\right] + \frac{1}{I_y} U_\theta \\
\ddot{\psi} \cong \dot{r} &= \frac{1}{I_z}\left[M_{gyro,3} + qp\left(I_x - I_y\right)\right] + \frac{1}{I_z} U_\psi \\
\ddot{z} \cong \dot{w} &= \frac{1}{m}\left[-F_{\text{drag}} s_\alpha - F_{\text{lift}} c_\alpha \right. \\
&\qquad \left. + mg c_\phi c_\theta + m\left(qu - pv\right)\right] + \frac{1}{m} U_z
\end{aligned} \tag{15}
$$

For the state-vector $\eta(t) = \begin{bmatrix}\phi & \dot{\phi} & \theta & \dot{\theta} & \psi & \dot{\psi} & z & \dot{z}\end{bmatrix}^T$ and input vector $\mu(t) = \begin{bmatrix}U_\phi & U_\theta & U_\psi & U_z\end{bmatrix}^T$, nonlinear state-space model can be written as

$$
\dot{\eta}(t) = A_1 \eta(t) + B_1\left[\mu(t) + f_1(\eta, t)\right] \tag{16}
$$

where the system matrix A and input matrix B are given as

$$
\begin{aligned}
A_1 &= \text{diag}\left(\begin{bmatrix}0 & 1\\ 0 & 0\end{bmatrix}, \begin{bmatrix}0 & 1\\ 0 & 0\end{bmatrix}, \begin{bmatrix}0 & 1\\ 0 & 0\end{bmatrix}, \begin{bmatrix}0 & 1\\ 0 & 0\end{bmatrix}\right) \\
B_1 &= \text{diag}\left(\begin{bmatrix}0\\ \frac{1}{I_x}\end{bmatrix}, \begin{bmatrix}0\\ \frac{1}{I_y}\end{bmatrix}, \begin{bmatrix}0\\ \frac{1}{I_z}\end{bmatrix}, \begin{bmatrix}0\\ \frac{1}{m}\end{bmatrix}\right) \\
f_1 &= \begin{bmatrix} M_{gyro,1} + qr\left(I_y - I_z\right) \\ M_{gyro,2} + M_{pitch} + pr\left(I_z - I_x\right) \\ M_{gyro,3} + qp\left(I_x - I_y\right) \\ -F_{\text{drag}} s_\alpha - F_{\text{lift}} c_\alpha + mg c_\phi c_\theta + m\left(qu - pv\right)\end{bmatrix}
\end{aligned}
$$

We assume that input matrix B_1 is unknown and it can be written as $B_1 = D_1 \Lambda_1$ where unknown control effectiveness matrix Λ_1 is a diagonal matrix with positive entries. Estimation of the unknown function $f_1(\eta, t)$ is denoted as $\hat{f}_1(\eta, t)$ and is given by

$$
\hat{f}_1(\eta, t) = \begin{bmatrix} \widehat{M}_{gyro,1} + qr\left(\widehat{I}_y - \widehat{I}_z\right) \\ \widehat{M}_{gyro,2} + \widehat{M}_{pitch} + pr\left(\widehat{I}_z - \widehat{I}_x\right) \\ \widehat{M}_{gyro,3} + qp\left(\widehat{I}_x - \widehat{I}_y\right) \\ -\widehat{F}_{\text{lift}} + m_o g c_\phi c_\theta + m_o\left(qu - pv\right)\end{bmatrix}
$$

where it is assumed that

$$
f_1(\eta, t) = \hat{f}_1(\eta, t) + W^T(t)\sigma(\eta) + \varepsilon(\eta)
$$

with $\|\varepsilon(\eta)\| \leq \bar{\varepsilon}$, $\forall \eta \in \mathcal{D}_\eta$ for a sufficiently large compact set $\mathcal{D}_\eta$. Then, we design the control input $\mu(t)$ as

$$
\mu(t) = \mu_{\text{ad}}(t) - \hat{f}(\eta, t)
$$

With these information, manipulating Equation 16 yields

$$
\begin{aligned}
\dot{\eta}(t) =& A_m \eta(t) + B_m r(t) \\
&+ D_1 \Lambda_1\left[\mu_{\text{ad}}(t) + \overline{W}^T(t)\overline{\sigma}(\eta, t) + \varepsilon(\eta)\right]
\end{aligned} \tag{17}
$$

where $\overline{W}^T(t) \triangleq \begin{bmatrix}W^T(t) & \Lambda_1^{-1} K_\eta & -\Lambda_1^{-1} K_r\end{bmatrix}$, $\overline{\sigma}(\eta, t) \triangleq \begin{bmatrix}\sigma^T(\eta) & \eta^T(t) & r^T(t)\end{bmatrix}^T$, and $A_m \triangleq A_1 - D_1 K_\eta$, $B_m \triangleq D_1 K_r$. Then, adaptive input $\mu_{\text{ad}}(t)$ is

$$
\mu_{\text{ad}}(t) = -\widehat{\overline{W}}^T(t)\overline{\sigma}(\eta, t)
$$

which yields

$$
\begin{aligned}
\dot{\eta}(t) =& A_m \eta(t) + B_m r(t) \\
&+ D_1 \Lambda_1\left[\widetilde{\overline{W}}^T(t)\overline{\sigma}(\eta, t) + \varepsilon(\eta)\right]
\end{aligned} \tag{18}
$$

with $\widetilde{\overline{W}}(t) \triangleq \overline{W}(t) - \widehat{\overline{W}}(t)$.

Now, we define the reference model

$$
\dot{\eta}_m(t) = A_m \eta_m(t) + B_m r(t)
$$

Let $e_a(t) \triangleq \eta_m(t) - \eta(t)$ be the tracking error. Then, its dynamics becomes

$$
\dot{e}_a(t) = A_m e_a(t) - D_1 \Lambda_1\left[\widetilde{\overline{W}}^T(t)\overline{\sigma}(\eta, t) + \varepsilon(\eta)\right] \tag{19}
$$

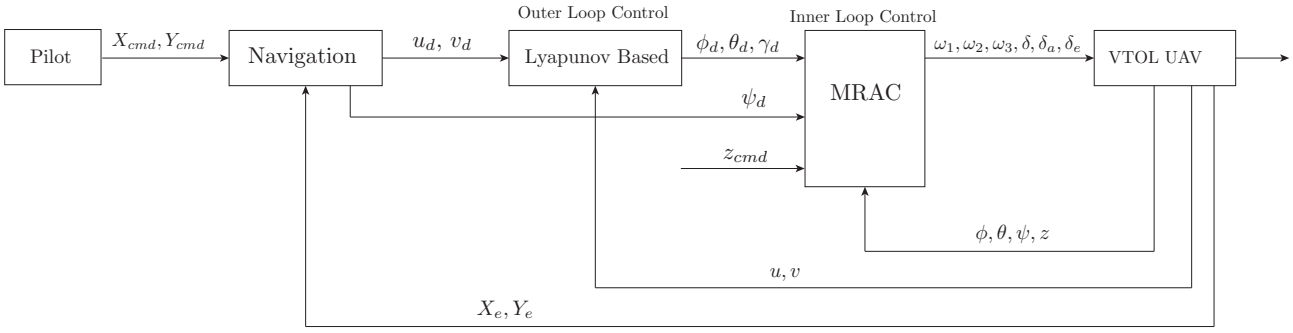

Figure 12: Block Diagram for Position Control Architecture

Weight update law is given by

$$\begin{aligned}\dot{\widehat{W}}(t) =& -\Gamma_1 \|e_a\|^2 \overline{\sigma}(\eta,t) e_a^T(t) P_1 D_1 \\ & -\Gamma_1\Gamma_2\left(\widehat{\overline{W}}(t) - \widehat{\overline{W}}_f(t)\right) \\ \dot{\widehat{W}}_f(t) =& \Gamma_f\left(\widehat{\overline{W}}(t) - \widehat{\overline{W}}_f(t)\right) - \Gamma_f\Gamma_4\left(\widehat{\overline{W}}_f(t) - W_0\right) \\ =& \Gamma_f\left(\widetilde{\overline{W}}_f(t) - \widetilde{\overline{W}}(t)\right) - \Gamma_f\Gamma_4\left(\widehat{\overline{W}}_f(t) - W_0\right)\end{aligned} \tag{20}$$

where W_0 is pre-selected weight chosen by the designer and $\widetilde{\overline{W}}_f(t) \triangleq \overline{W}(t) - \widehat{\overline{W}}_f(t)$.

Remark 1. *With the following Lyapunov function*

$$\begin{aligned}\mathcal{V}_1(t) =& \frac{1}{\lambda_{\max}(P_1)}\left(e_a^T P_1 e_a\right)^2 \\ &+ tr\left[\left(\widetilde{\overline{W}}\Lambda_1^{1/2}\right)^T \Gamma_1^{-1}\left(\widetilde{\overline{W}}\Lambda_1^{1/2}\right)\right] \\ &+ tr\left(\widetilde{\overline{W}}_f^T(t)\Gamma_f^{-1}\widetilde{\overline{W}}_f(t)\right)\end{aligned} \tag{21}$$

it can be shown that the tracking error $e(t)$ and weight estimation error $\widetilde{\overline{W}}$ are bounded. Since reference model state $\eta(t)$ and unknown weight matrix $\overline{W}(t)$ are known to be bounded, system states $\eta(t)$ and estimated weight matrix $\widehat{\overline{W}}(t)$ are guaranteed to be bounded.

6.2. Control Allocation

Recall the control input $\mu(t)$

$$\begin{aligned}\mu(t) =& \mu_{\text{ad}}(t) - \hat{f}(\eta,t) = \begin{bmatrix} U_\phi \\ U_\theta \\ U_\psi \\ U_z \end{bmatrix} \\ =& \begin{bmatrix} c_{tf} l_w u_1 c_\gamma - c_{qf} u_1 s_\gamma + M_{x,a} \\ c_{tf} l_1 u_2 c_\gamma - c_{ta} l_2 u_3 - c_{qa} u_4 + M_{y,e} \\ c_{tf} l_w u_1 s_\gamma - c_{ta} l_2 u_4 + c_{qf} u_1 c_\gamma + c_{qa} u_3 \\ -c_{tf} u_2 c_\gamma - c_{ta} u_3 \end{bmatrix}\end{aligned} \tag{22}$$

Both pitch and roll attitude can be controlled either using control surface deflections and differential thrust of motors with related tilt angles. Obviously, this is valid if the velocity V_∞ is relatively large. At this point, we introduce a parameter k_{tr} that mixes the control surface inputs and propulsive inputs during the transition maneuver. For low airspeed, we use only propulsive inputs to control the attitude whereas we use the control surface deflections at high airspeed. In between, however, we mix these to class of inputs using k_{tr}. Noting that $V_{tr,0}$ and $V_{tr,1}$ are user-selected velocities that correspond the aforementioned low and high airspeed (resp.), control mixer parameter k_{tr} is given as

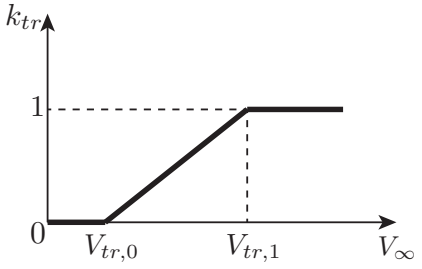

Figure 13: Control Mixer Parameter

We separate two class of inputs as follows:

$$\begin{aligned}\underbrace{c_{tf} l_w u_1 c_\gamma - c_{qf} u_1 s_\gamma}_{=(1-k_{tr})U_\phi} + \underbrace{M_{x,a}}_{=k_{tr}U_\phi} &= U_\phi \\ \underbrace{c_{tf} l_1 u_2 c_\gamma - c_{ta} l_2 u_3 - c_{qa} u_4}_{=(1-k_{tr})U_\theta} + \underbrace{M_{y,e}}_{=k_{tr}U_\theta} &= U_\theta\end{aligned} \tag{23}$$

Then, the actual control inputs ω_i for $i = 1, 2, 3$, aft motor tilt angle δ, and control surface deflections δ_a and δ_e can be obtained as

$$\begin{aligned}\omega_1 &= \sqrt{\frac{u_1+u_2}{2}}, \quad \omega_2 = \sqrt{\frac{u_2-u_1}{2}} \\ \omega_3 &= \sqrt[1/4]{u_3^2+u_4^2}, \quad \delta = atan_2(u_4,u_3) \\ \delta_a &= \frac{2k_{tr}U_\phi}{\rho_\infty V_\infty^2 S_{ref}\bar{c}\, C_{M_a}}, \quad \delta_e = \frac{2k_{tr}U_\theta}{\rho_\infty V_\infty^2 S_{ref}\bar{c}\, C_{M_e}}\end{aligned} \tag{24}$$

where u_i's are obtained from

$$\begin{bmatrix} u_1 \\ u_2 \\ u_3 \\ u_4 \end{bmatrix} = H^{-1} \begin{bmatrix} (1-k_{tr})U_\phi \\ (1-k_{tr})U_\theta \\ U_\psi \\ U_z \end{bmatrix} \tag{25}$$

with matrix H being

$$H = \begin{bmatrix} c_{tf} l_w c_\gamma - c_{qf} s_\gamma & 0 & 0 & 0 \\ 0 & c_{tf} l_1 c_\gamma & -c_{ta} l_2 & -c_{qa} \\ c_{tf} l_w s_\gamma + c_{qf} c_\gamma & 0 & c_{qa} & -c_{ta} l_2 \\ 0 & -c_{tf} c_\gamma & -c_{ta} & 0 \end{bmatrix} \tag{26}$$

Remark 2. *One can realize that matrix H becomes singular when front tilt angle $\gamma = \tan^{-1}\left(\frac{c_{tf} l_w}{c_{qf}}\right)$. Typically, thrust coefficient is 100 times larger torque coefficient. Then, for a mini UAV, tilt angle γ that makes H singular is around $\gamma = 85^o$. We consider that the airspeed is sufficiently large at $\gamma = 85^o$ so that we can eliminate the singularity occurred in roll dynamics by enforcing the constraint $\omega_1 = \omega_2$.*

6.3. Outer Loop Controller Design

Once the stable inner loop controller is designed, we move onto outer loop control that generates the desired commands for the inner loop. In this part, we will make use of the Lyapunov control theory to design a stable outer control loop. First, we define the state-vector as $\zeta(t) = \begin{bmatrix} u & v \end{bmatrix}^T$. Let $u_d(t)$ and $v_d(t)$ be the desired velocities in x_b and y_b directions, respectively. Let $e_u(t) \triangleq u_d(t) - u(t)$ be the velocity tracking error. In addition, let $U_x \triangleq (c_{tf} s_\gamma u_2 - mgs_\theta)$ and $U_y \triangleq (c_{ta} u_4 + mgs_\phi c_\theta)$. Then, translational equations of motion can be written as

$$\begin{aligned} \dot{u} &= \frac{1}{m}\left[U_x - F_{\text{drag}} c_\alpha + F_{\text{lift}} s_\alpha + m(rv - qw)\right] \\ \dot{v} &= \frac{1}{m}\left[U_y + m(pw - ru)\right] \end{aligned} \tag{27}$$

We design pseudo-controls U_x and U_y as follows

$$\begin{aligned} U_x =& \widehat{F}_{\text{drag}} c_\alpha - \widehat{F}_{\text{lift}} s_\alpha - m_o(rv - qw) \\ &+ m_o \dot{u}_d(t) + k_1 e_u(t) \\ U_y =& -m_o(pw - ru) + m_o \dot{v}_d(t) + k_2 e_v(t) \end{aligned} \tag{28}$$

Remark 3. *With these pseudo-controls, it can be shown that the signals $e_u(t)$ and $e_v(t)$ are bounded. Thus, boundedness of desired signals $u_d(t)$ and $v_d(t)$ ensures the Lyapunov stability of the system states $u(t)$ and $v(t)$.*

Recall the relations for U_x and U_y

$$\begin{aligned} U_x =& c_{tf} s_\gamma u_2 - mg\sin(\theta) \\ U_y =& c_{ta} u_4 + mg\sin(\phi)\cos(\theta) \end{aligned} \tag{29}$$

At this point, we make the following trick to adjust the desired pitch angle during transition

$$\begin{aligned} U_x =& c_{tf} s_\gamma u_2 - mgs_\theta \pm mg\sin(\theta_o) \\ =& \underbrace{c_{tf} s_\gamma u_2 - mg\sin(\theta_o)}_{k_{tr} U_x} + \underbrace{mg\sin(\theta_o) - mgs_\theta}_{(1-k_{tr})U_x} \end{aligned} \tag{30}$$

Then, desired pitch and tilt angles become

$$\begin{aligned} \gamma_d =& \sin^{-1}\left(\frac{k_{tr} U_x + m_o g \sin(\theta_o)}{c_{tf} u_2}\right) \\ \theta_d =& \sin^{-1}\left(\frac{(k_{tr}-1)U_x}{m_o g} + \sin(\theta_o)\right) \\ \phi_d =& \sin^{-1}\left(\frac{U_y - c_{ta} u_4}{mg\cos(\theta)}\right) \end{aligned} \tag{31}$$

Assuming the angle of attack, pitch and roll angles are small, we may write the angle of attack that generates the desired lift as follows

$$\alpha_d = \frac{2m_o g}{\rho V_\infty^2 S_{ref} C_{L_\alpha}} \tag{32}$$

However, desired angle of attack at low airspeed becomes unbounded. So, we bound the desired angle of attack to stay in the linear region

$$\alpha_d = \text{sat}\left(\frac{2m_o g}{\rho V_\infty^2 S_{ref} C_{L_\alpha}}; \pm 0.15 \text{ rad}\right) \tag{33}$$

Flight path angle can be calculated as

$$\gamma_{\text{fp}} = \tan^{-1}\left(\frac{\Delta Z_e}{\Delta X_e}\right) = \tan^{-1}\left(\frac{V_z}{V_x}\right) \tag{34}$$

where ΔZ_e and ΔX_e are distances traveled in small time interval Δt in the earth-fixed frame axes of Z_e and X_e, respectively. Then, pitch attitude offset θ_o can be obtained as

$$\begin{aligned} \theta_o &= \alpha_d + \gamma_{\text{fp}} \\ &= \text{sat}\left(\frac{2m_o g}{\rho V_\infty^2 S_{ref} C_{L_\alpha}}\right) + \tan^{-1}\left(\frac{V_z}{V_x}\right) \end{aligned} \tag{35}$$

6.4. Navigation

Note that desired yaw angle is still to be determined. Furthermore, position controller is based on equation of motion expressed in body frame $\mathcal{F}_b$. However, position to be tracked is defined in navigation frame or inertial frame in general. In this section, we construct a navigation algorithm that extracts desired position in body frame and desired heading from the given desired navigational position. Let $X_{e_d}(t)$ and $Y_{e_d}(t)$ be the desired path on the horizontal navigation plane.

Then, we transform the inertial position to the body frame by

$$\begin{bmatrix} x_{b_d} \\ y_{b_d} \end{bmatrix} = \begin{bmatrix} \cos(\psi) & \sin(\psi) \\ -\sin(\psi) & \cos(\psi) \end{bmatrix} \begin{bmatrix} X_{e_d} \\ Y_{e_d} \end{bmatrix}$$

where x_{b_d} and y_{b_d} are the components of desired position vector in body frame $\mathcal{F}_b$.
In addition, desired yaw angle ψ_d is determined as

$$\psi_d = atan_2\left(Y_{e_d} - Y_e, X_{e_d} - X_e\right)$$

Finally, having generated the desired positions in body frame axes x_b and y_b, desired body velocities $u_d(t)$ and $v_d(t)$ are obtained through PD-controller. Block diagram for navigation and PD-control structure is illustrated in Figure 14.

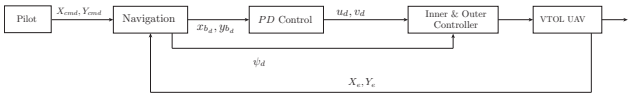

Figure 14: Navigation and the Most Outer Control

7. SIMULATION RESULTS

Desired inertial position is commanded to the aircraft through a ground control station. The scenario is as follows: Aircraft first takes off and climbs vertically up to 30 meters. Once the desired altitude is achieved, aircraft is commanded to fly through a checkpoint of $(2500, 0)$ in meters. Then, front rotors tilt forward to accelerate as figure 18 illustrates. Aircraft flies in fixed wing configuration for a while to reach the first checkpoint. During this period, aft front nearly stops and front two rotors reduce to half of their vertical flight values. Once the first checkpoint is reached, desired heading angle is determined to be 90^o degrees (see Figure 15) to direct the aircraft through the second checkpoint which is $(2500, 2500)$ in meters. During this 90 degree-maneuver, aircraft slows down and bring front rotor upward. This process is repeated for 4 times to complete an exact square trajectory. Eventually, aircraft hovers at the initial position at 30 meters altitude. It can be seen that the front rotors stay upward and aft rotor rotates at its %70 capacity (see Figure 17).

Transition corridor of the UAV is obtained by GAVM trimmer. Velocity sweep analyses are conducted for different tilt angles. Lift to drag ratio and required power contours are plotted for the transition corridor in Figure 20 and Figure 21 with the controller flight simulation results.

Results show that the most efficient transition maneuver is successfully conducted for angle of attack at which L/D becomes maximum. If the purpose is comfort zero pitch can be achieved but the maneuver becomes less efficient and level flight cannot be sustained for low airspeeds (i.e. out of the corridor) which results in small amount of altitude loss.

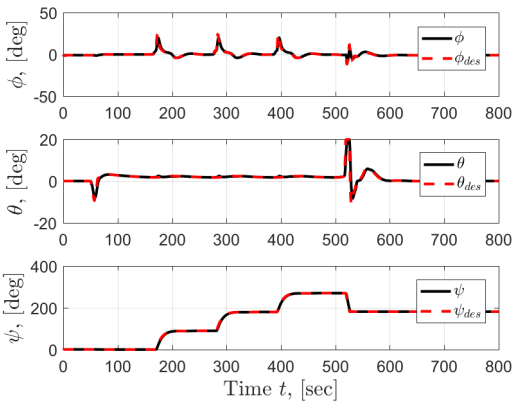

Figure 15: Attitude Tracking Performance

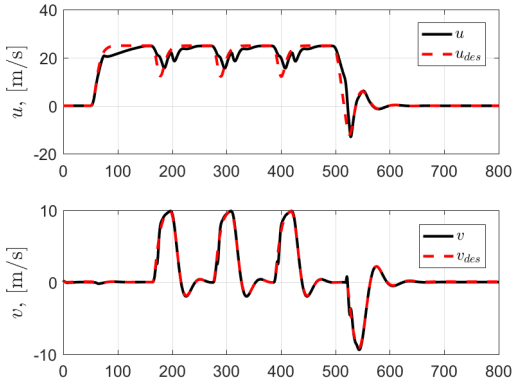

Figure 16: Velocity Components in Body Frame $\mathcal{F}_b$

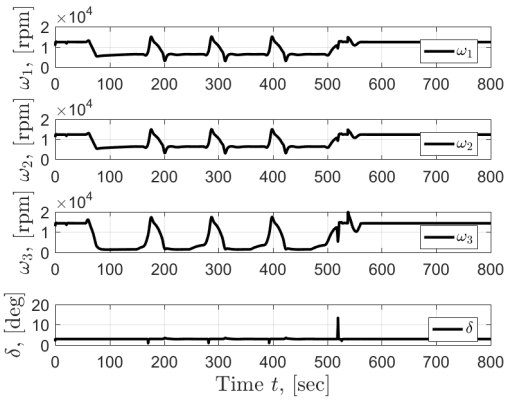

Figure 17: Propulsive Control Inputs

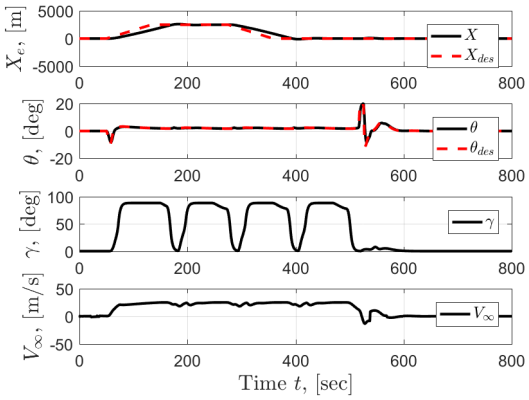

Figure 18: Transition Maneuver

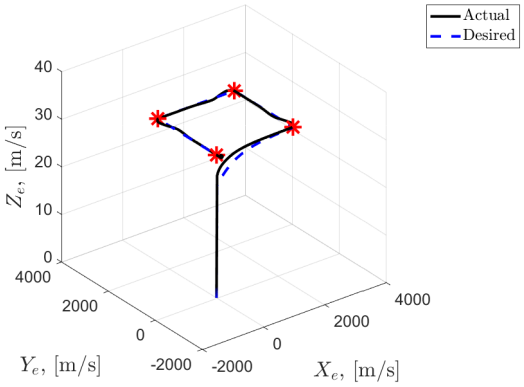

Figure 19: 3-dimensional Trajectory in Inertial Frame

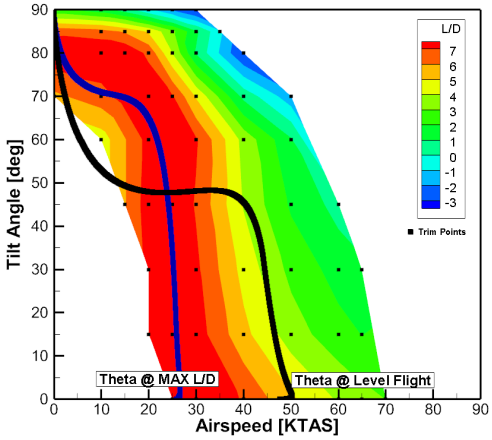

Figure 20: Transition simulation and GAVM L/D contours

.

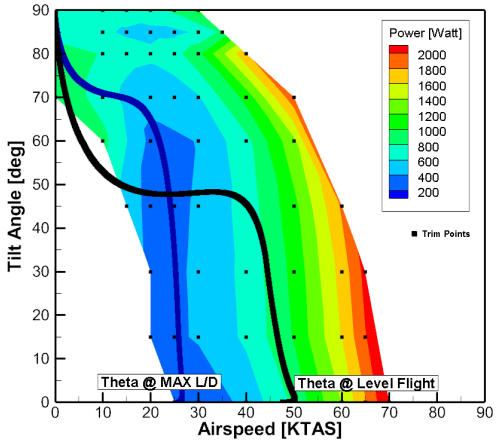

Figure 21: Transition simulation and GAVM required power contours

8. CONCLUSION

In this work, an optimal adaptive controller is designed for a vertical take-off and landing tilt-prop UAV manufactured in METU Aerospace Engineering Department. This work deals with fully automated transition control of a Tilt-Prop UAV including uncertainties in system modeling and system parameters. In addition, transition controller performs optimal transition in terms of required power without any a-priori information from transition corridor. Actually, the controller designed in this work is able to perform transition for any path defined in the transition corridor with a desired time. Therefore, transition maneuver can be performed by using agile, comfort, or efficient paths according to the mission requirements. Overall, the success of the GAVM trimmer and the transition controller is aimed to be proven by flight tests as future work.

REFERENCES

[1] M. D. Maisel, D. J. Giulianetti, and D. C. Dugan. The history of the xv-15 tilt rotor research aircraft: from concept to flight. 2000.

[2] Ximin Lyu, Haowei Gu, Jinni Zhou, Zexiang Li, Shaojie Shen, and Fu Zhang. A hierarchical control approach for a quadrotor tail-sitter vtol uav and experimental verification. *IEEE/RSJ International Conference on Intelligent Robots and Systems*, 2017.

[3] Jinni Zhou, Ximin Lyu, Zexiang Li, Shaojie Shen, and Fu Zhang. A unified control method for quadrotor tail-sitter uavs in all flight modes: Hover, transition, and level flight. In *Proc. of the*

IEEE/RSJ Intl. Conf. on Intell. Robots and Syst. IEEE, 2017.

[4] Boyang Li, Weifeng Zhou, Jingxuan Sun, Chihyung Wen, and Chihkeng Chen. Model predictive control for path tracking of a vtol tailsitter uav in an hil simulation environment. In *2018 AIAA Modeling and Simulation Technologies Conference*, page 1919, 2018.

[5] Zhong Liu, Didier Theilliol, Liying Yang, Yuqing He, and Jianda Han. Transition control of tilt rotor unmanned aerial vehicle based on multi-model adaptive method. In *Unmanned Aircraft Systems (ICUAS), 2017 International Conference on*, pages 560–566. IEEE, 2017.

[6] Ertuğrul Çetinsoy, Serhat Dikyar, Cevdet Hançer, KT Oner, E Sirimoglu, M Unel, and MF Aksit. Design and construction of a novel quad tilt-wing uav. *Mechatronics*, 22(6):723–745, 2012.

[7] Gerardo Flores and Rogelio Lozano. A nonlinear control law for hover to level flight for the quad tilt-rotor uav. In *19th World Congress The International Federation of Automatic Control (IFAC 2014)*, pages 11055–11059, 2014.

[8] Yildiray Yildiz, Mustafa Unel, and Ahmet Eren Demirel. Nonlinear hierarchical control of a quad tilt-wing uav: An adaptive control approach. *International Journal of Adaptive Control and Signal Processing*, 31(9):1245–1264, 2017.

[9] Jacob Apkarian. Pitch-decoupled vtol/fw aircraft: First flights. In *Research, Education and Development of Unmanned Aerial Systems (RED-UAS), 2017 Workshop on*, pages 258–263. IEEE, 2017.

[10] Jose A Bautista, Antonio Osorio, and Rogelio Lozano. Modeling and analysis of a tricopter/flying-wing convertible uav with tilt-rotors. In *Unmanned Aircraft Systems (ICUAS), 2017 International Conference on*, pages 672–681. IEEE, 2017.

[11] Stephen Carlson. A hybrid tricopter/flying-wing vtol uav. In *52nd Aerospace Sciences Meeting*, page 0016, 2014.

[12] Chen Chao, Shen Lincheng, Zhang Daibing, and Zhang Jiyang. Mathematical modeling and control of a tiltrotor uav. In *Information and Automation (ICIA), 2016 IEEE International Conference on*. IEEE, 2016.

[13] Chao Chen, Jiyang Zhang, Daibing Zhang, and Lincheng Shen. Control and flight test of a tilt-rotor unmanned aerial vehicle. *International Journal of Advanced Robotic Systems*, 14(1):1729881416678141, 2017.

[14] Philipp Hartmann, Carsten Meyer, and Dieter Moormann. Unified velocity control and flight state transition of unmanned tilt-wing aircraft. *Journal of Guidance, Control, and Dynamics*, 40(6):1348–1359, 2017.

[15] J Holsten and D Moormann. Flight control law design criteria for the transition phase for a tiltwing aircraft using multi-objective parameter synthesis. *CEAS Aeronautical Journal*, 6(1):17–30, 2015.

[16] Pedro Casau, David Cabecinhas, and Carlos Silvestre. Autonomous transition flight for a vertical take-off and landing aircraft. In *Decision and Control and European Control Conference (CDC-ECC), 2011 50th IEEE Conference on*, pages 3974–3979. IEEE, 2011.

[17] Li Yu, Daibing Zhang, and Jiyang Zhang. Transition flight modeling and control of a novel tilt tri-rotor uav. In *Information and Automation (ICIA), 2017 IEEE International Conference on*, pages 983–988. IEEE, 2017.

[18] Gerardo Flores and Rogelio Lozano. Transition flight control of the quad-tilting rotor convertible mav. In *Unmanned Aircraft Systems (ICUAS), 2013 International Conference on*, pages 789–794. IEEE, 2013.

[19] Sanghyuk Park, John Deyst, and Jonathan How. A new nonlinear guidance logic for trajectory tracking. In *AIAA guidance, navigation, and control conference and exhibit*, page 4900, 2004.

[20] Daniel Mellinger and Vijay Kumar. Minimum snap trajectory generation and control for quadrotors. In *Robotics and Automation (ICRA), 2011 IEEE International Conference on*, pages 2520–2525. IEEE, 2011.

[21] Zafer Öznalbant and Mehmet Ş Kavsaoğlu. Flight control and flight experiments of a tilt-propeller vtol uav. *Transactions of the Institute of Measurement and Control*, 40(8):2454–2465, 2018.

[22] Yih Tang Yeo and Hugh H Liu. Transition control of a tilt-rotor vtol uav. In *2018 AIAA Guidance, Navigation, and Control Conference*, page 1848, 2018.

[23] Zhong Liu, Yuqing He, Liying Yang, and Jianda Han. Control techniques of tilt rotor unmanned aerial vehicle systems: A review. *Chinese Journal of Aeronautics*, 30(1):135–148, 2017.

[24] L. Cevher. Control System Design and Implementation of a Tilt Rotor UAV. Master's thesis, Middle East Technical University, Turkey, 2018.

[25] M. Senipek. Development of an Object-Oriented Design, Analysis and Simulation Software for a Generic Air Vehicle. Master's thesis, Middle East Technical University, Turkey, 2017.

[26] A. S. Onen, L. Cevher, M. Senipek, T. Mutlu, O. Gungor, I. O. Uzunlar, D. F. Kurtulus, and O. Tekinalp. Modeling and controller design of a vtol uav. In *International Conference on Unmanned Aircraft Systems*, pages 329–337. IEEE, 2015.
[27] A. S. Onen, L. Cevher, T. Mutlu, O. Gungor, and O. Tekinalp. Dikey kalkis ve inis yapabilen iha'nin pervane itki sistemi ruzgar tuneli testleri. In *3. Ulusal Havacılıkta İleri Teknolojiler Konferansı*, 2014.
[28] M. Drela. Qprop formulation, June 2006.